Petroleum Science 19 (2022) 1125–1138

Contents lists available at ScienceDirect

Petroleum Science

journal homepage: www.keaipublishing.com/en/journals/petroleum-science

Original Paper

Characterization of the fracture compressibility and its permeability for shale under the effects of proppant embedment and compaction: A preliminary study

Jian-Hua Li [a, b, c], Bo-Bo Li [c, d, e, *], Qiao-Yun Cheng [c], Zheng Gao [c]

[a] Guangdong Provincial Key Laboratory of Deep Earth Sciences and Geothermal Energy Exploitation and Utilization, Institute of Deep Earth Sciences and Green Energy, College of Civil and Transportation Engineering, Shenzhen University, Shenzhen, 518060, Guangdong, China
[b] Shenzhen Key Laboratory of Deep Underground Engineering Sciences and Green Energy, Shenzhen University, Shenzhen, 518060, Guangdong, China
[c] College of Mining, Guizhou University, Guiyang, 550025, Guizhou, China
[d] Guizhou Key Laboratory of Comprehensive Utilization of Non-metallic Mineral Resources, Guiyang, 550025, Guizhou, China
[e] National & Local Joint Laboratory of Engineering for Effective Utilization of Regional Mineral Resources from Karst Areas, Guizhou University, Guiyang, 550025, Guizhou, China

ARTICLE INFO

Article history:
Received 15 July 2021
Accepted 8 December 2021
Available online 18 December 2021

Edited by Yan-Hua Sun

Keywords:
Shale
Fracture compressibility
Permeability
Hydraulic fracturing
Proppant embedment

ABSTRACT

Hydraulic fracturing technology plays a key role in improving the recovery rate of shale gas. The improvement of permeability in relation to hydraulic fracturing depends on changes brought about by the proppant on the fracture structure in reservoirs. Then it is of great significance to describe the microscopic changes during this process by means of an accurate theoretical model. In this study, based on the heterogeneity of shale fracture and the compaction and embedment of a proppant, we proposed a permeability model to examine the combined effects of a proppant and stress to describe the change mechanism in permeability. Further, changes in fracture width and porosity were considered, and a calculation model of fracture compressibility under proppant compaction and embedment was proposed. The difference from previous studies is that the compressibility and permeability of supported fractures can be further quantified and analyzed by this model. Moreover, its rationality was verified by publicly released test data. The results show that, the compressive effect of stress and the embedding of proppant both have a negative impact on shale permeability.
© 2021 The Authors. Publishing services by Elsevier B.V. on behalf of KeAi Communications Co. Ltd. This is an open access article under the CC BY-NC-ND license (http://creativecommons.org/licenses/by-nc-nd/4.0/).

1. Introduction

In recent years, unconventional oil and gas resources, dominated by shale gas, have gradually attracted people's attention (Tan et al., 2017). Owing to its huge reserves, many countries have gradually introduced commercial production (McGlade et al., 2013). However, in the *in-situ* environment, the permeability in shale reservoirs is extremely low (Lv et al., 2020; Zhang et al., 2021). Because of the extremely low permeability in shale reservoirs, permeability improvement technologies have been implemented in order to improve gas recovery. At present, the main technology for improving shale gas recovery is the multi-stage hydraulic fracturing technology of horizontal wells (Estrada and Bhamidimarri, 2016; Zhou et al., 2019). However, in this process, smaller proppant particles must be injected first, and then larger proppant particles (Liu et al., 2021). Due to the small movement aperture of natural fractures in the reservoir, micro proppants are needed to support them (Gale et al., 2014; Hon et al., 2019). At this time, the so-called hierarchical proppant injection or hierarchical proppant placement generally refers to partial single-layer placement of microproppants (Khanna et al., 2013; Keshavarza et al., 2016). Because the secondary and tertiary fractures are too narrow to fill the proppant filler (Warpinski et al., 2008), the implementation effect of hydraulic fracturing technology depends on the supporting effect of proppants on reservoir fractures (Keshavarza et al., 2016). The embedment of proppant causes permeability changes by changing the width of fractures in the shale reservoir, and permeability has been shown to be one of the key parameters that determines the ability of gas to flow in the reservoir (Wei and Xia, 2017; Yang et al., 2015). In

* Corresponding author. College of Mining, Guizhou University, Guiyang, 550025, Guizhou, China.
E-mail address: bbli@gzu.edu.cn (B.-B. Li).

https://doi.org/10.1016/j.petsci.2021.12.021
1995-8226/© 2021 The Authors. Publishing services by Elsevier B.V. on behalf of KeAi Communications Co. Ltd. This is an open access article under the CC BY-NC-ND license (http://creativecommons.org/licenses/by-nc-nd/4.0/).

addition, changes in permeability also depend on fracture compressibility (Tan et al., 2019). Because fracture compressibility is a key parameter for modeling fracture closure and for estimating fracture volume changes in fractured reservoirs (Xu et al., 2020), it also plays an important role in predicting oil and gas production in fractured reservoirs and in estimating the oil/gas recovery. Therefore, when evaluating the implementation effect of hydraulic fracturing technology, a first step should be to evaluate the change mechanism relating to the permeability and the fracture compressibility coefficient during proppant compaction and embedding.

When discussing the effect of hydraulic fracturing on the anti-permeability of the reservoir, it is of great significance to measure the supported fracture permeability. In this process, permeability changes depend on stress, the rock mechanical properties of the reservoir and the properties of the proppant (Ahamed et al., 2019; Bandara et al., 2019; Chen et al., 2017). Previous studies have shown that there was a negative exponential functional relationship between shale permeability and stress (Chen et al., 2015, 2019). As stress increased, shale permeability gradually decreased. However, while the fracture was supported by the proppant, the embedding depth of the proppant and the deformation of the proppant determined the change in permeability (Ahamed et al., 2021). Moreover, the type, size and packing form of the proppant would affect the width of the fracture (Xu et al., 2020). Compared with the original sample, the permeability in the shale reservoir embedded with proppant would be greatly improved (Hou and Elsworth. 2021). And the concentration of the proppant was also related to permeability (Wen et al., 2007). Normally, proppants with smaller particle sizes have shown a greater pressure-bearing capacity, but their effect on permeability improvement was lower than those with larger particle sizes (Tan et al., 2017). In addition, in rock reservoirs, the compaction and embedment of proppants in fractures have also been seen as an important issue, which was one of the key factors that resulted in permeability changes. However, the embedding depth of a proppant was difficult to quantify through laboratory experiments. Consequently, an accurate theoretical model would be of great value for the quantitative analysis of proppant embedding depth. Chen et al. (2017) proposed a power-law relationship model between embedding depth and stress to describe changes in proppant embedding depth through the functional relationship between proppant embedding depth and effective stress. For single-layer and multi-layer proppant-supported rock formations, Li et al. (2015) proposed a calculation model to describe variations in proppant embedding depth. That model assumed that the proppant was evenly spread in the rock formation. Guo and Liu (2012) used the elastic theory based on contact mechanics, while ignoring the surface roughness, and possible proppant crushing, and secondary fracturing of the fracture well, and proposed a proppant embedding depth calculation model. Meanwhile, the change of permeability is related to the change of fracture width, which is very important for the simulation and prediction of reservoir permeability (Liu et al., 2017; Wang et al., 2021). For adsorptive media such as shale or coal, the evolution of its permeability is mostly restricted by the gas adsorption effect and stress compression (Pan and Connell. 2012; Wei et al., 2019; Zeng et al., 2020a, 2020b). In view of the effect of stress, Seidle and Huitt (1995) derived an exponential function permeability model based on the classic matchstick model. Robertson and Christiansen (2006) incorporated the influence of adsorption strain into the permeability model, and further quantitatively analyzed the influence of gas adsorption and stress on permeability. Based on the poroelastic equation, Liu et al. (2011) used the stress and strain in coal as a bridge to derive the cubic relationship between fracture strain and permeability, and simulated the seepage law of coal and rock. In recent years, in view of the influence of the time effect and the internal expansion effect caused by the adsorption strain, Zeng et al. (2021) proposed a permeability model based on the linear relationship between the matrix expansion strain and the adsorbed gas content to analyze the evolution of multiple permeability caused by sorption. Wei et al. (2021) analyzed the influence of matrix and fracture balance time lag on the evolution of coal permeability, and the proposed permeability model predicts the change of coal permeability with time. However, under the support of proppant, the evolution of permeability of rock mainly depends on the influence of the embedding depth of proppant and the change of the filling layer on the fracture width. Xu et al. (2020) proposed a cleat compressibility coefficient considering the depth of proppant embedding based on the Hertzian contact theory, and further discussed the seepage characteristics of supporting fractures. Then the cleat compressibility and permeability equation of proppant-supported fractures were further proposed. On the basis of the power law relationship between proppant embedding depth and stress, Chen et al. (2016) constructed a cubic permeability model considering the effects of proppant and stress. Zhang and Hou (2016) constructed a permeability model to describe the conductivity of rock reservoirs by analyzing the influence of proppant on fractured channels, porosity and tortuosity.

Permeability is one of the key parameters for evaluating unconventional oil and gas production (Gao et al., 2020; Zeng et al., 2020a, 2020b). In which, fracture closure and fracture volume changes in fractured reservoirs can be characterized by the fracture compressibility C_f (Seidle et al., 1992; Shi and Durucan, 2010). The accuracy of fracture compressibility, as a key input, is critical for accurately predicting permeability and gas production behavior. Previous studies have shown that the fracture compressibility in rock reservoirs was not constant (Mckee et al., 1988; Chen et al., 2016), as the fracture compressibility changed with effective stress. Further, changes in fracture compressibility were also affected by some internal factors (for example, sample maturity and pore structure characteristics), and external factors (for example, the buried depth of the reservoir, humidity, temperature, fluid type, stress state, pore pressure and boundary conditions) (Cao et al., 2016; Feng et al., 2016; Meng and Li, 2013). Moreover, the test results of Meng and Li (2013) showed that fracture compressibility increased with an increase in the maximum vitrinite reflectivity. Because of the anisotropic structure of shale reservoir fractures, compressibility in all directions were also different (Tan et al., 2017). However, it is difficult to measure fracture compressibility owing to the extremely low porosity of unconventional reservoirs. Therefore, it was considered important to estimate or calculate fracture compressibility in a more precise way. At present, test data were usually directly fitted to obtain fracture compressibility, but also to obtain average value (Chen et al., 2016). In order to characterize the change law of compressibility with stress, Mckee et al. (1988) assumed for the first time that the compressibility of fractures decreased exponentially with stress, and proposed a calculation model for compressibility (Mckee et al., 1988). In it, the fracture compressibility was related to the fracture structure, so the fracture compressibility could also be further characterized by the fractal dimension (Cao et al., 2016). Based on the NMR test and an analysis of the seepage space, Li et al. (2013) further deduced a calculation method for the fracture compressibility coefficient during the stress change process (Li et al., 2013). Shale or coal was generally regarded as an elastomer, and the compressibility coefficient of the matrix part could be determined through experiments (Guo et al., 2014; Pei et al., 2018). In addition, there is a functional relationship between the matrix compressibility coefficient and the fracture compressibility coefficient (Pan et al., 2019; Zhu et al., 2018).

The compaction and embedding effect of a proppant determines the anti-reflection effect in hydraulic fracturing. The laying method of proppant in a fractured channel is single-layer or multi-layer, as

shown in Fig. 1. A proppant improves the width of the fracture through compaction and embedding, thereby affecting permeability. Aiming to reveal the influence of a proppant, Xu et al. (2020) analyzed the embedding depth of a proppant based on the Hertz contact model, and proposed a calculation model for the compressibility coefficient of supporting fractures based on changes in the fracture volume. However, the Hertz contact model might be improved to be ineffective when the proppant was placed in multiple layers. The deformation of the proppant will also cause changes in the packing layer. Therefore, considering the compaction and embedment effect of proppant, a new calculation method for compressibility for propped fractures was proposed. On this basis, a shale permeability model for supported fractures is further proposed. Different from previous studies, this study can be used to estimate and quantify the fracture compressibility changes of proppant-supported fractures. Meanwhile, the proposed model also includes the effect of the heterogeneity of rock fractures. Recently, considering the influence of gas pressure and effective stress on gas permeability in porous rocks (such as shale and coal), Pan et al. (2015) proposed a permeability model which combined effect of stress and slippage effect. Then the permeability model is successfully matched with the permeability test data of propped fractures by proppant in coal/shale (Wu et al., 2018; Tan et al., 2017, 018). In view of this, we also incorporated the slippage effect into the proposed permeability model. Therefore, the proposed permeability model also includes the effects of proppant compaction/embedding, fracture heterogeneity, and slippage effect. Among them, the rationality of the model can be verified through publicly released test data. Besides that, we also compared the changing laws of permeability and compressibility of supported fractures under different types of rocks, proppant with different elastic modulus, and different packing forms. This paper, as a preliminary study, has explored the permeability evolution and fracture compressibility coefficient of a single-layer proppant, and understood that the proppant was an elastic sphere in this study. In the next step of the study, we will further carry out more in-depth research, to consider the multi-layer placement of proppants and the elastoplastic changes in proppants. And through relevant experiments to explore further the influence of proppants on shale permeability in the process of hydraulic fracturing, in order to provide theoretical guidance for the implementation of hydraulic fracturing technology.

2. Modelling of shale permeability under the effect of single proppant embedment

2.1. Evolution mechanism of shale fractures under a single proppant embedment

There are complex fracture systems in natural shale. Previous studies have shown that fractures in shale are divided into soft and hard parts, which follow the two Hooke's laws, that is, Hooke's law based on natural strain and Hooke's law based on engineering strain (Liu et al., 2009) (as shown in Fig. 2).

When considering the soft and hard fracture systems in shale, the fracture width can normally be expressed as (Chen et al., 2012):

$$b = b_s + b_h \tag{1}$$

where b, b_s, b_h represent the current fracture widths of the entire rock, fractures (soft part), and matrix (hard part), respectively.

In the process of external stress change, shale fracture deformation is heterogeneous, whereas, in fracture deformation relating to the soft part, the relationship between stress and strain can be described by natural strain based Hooke's law (Liu et al., 2009; Shang et al., 2019):

$$d\sigma_e = K_s d\varepsilon_{vs} \tag{2}$$

where σ_e is the effective stress; K_s is the modulus of the soft part; and ε_{vs} is the volume strain of soft part.

Furthermore, the strain in the fracture can be described by the incremental change of the fracture as:

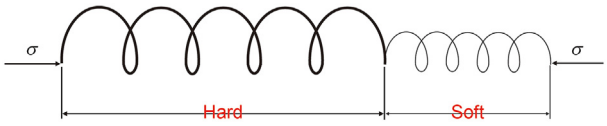


Fig. 2. Schematic diagram of fracture structure (after Liu et al., 2009).

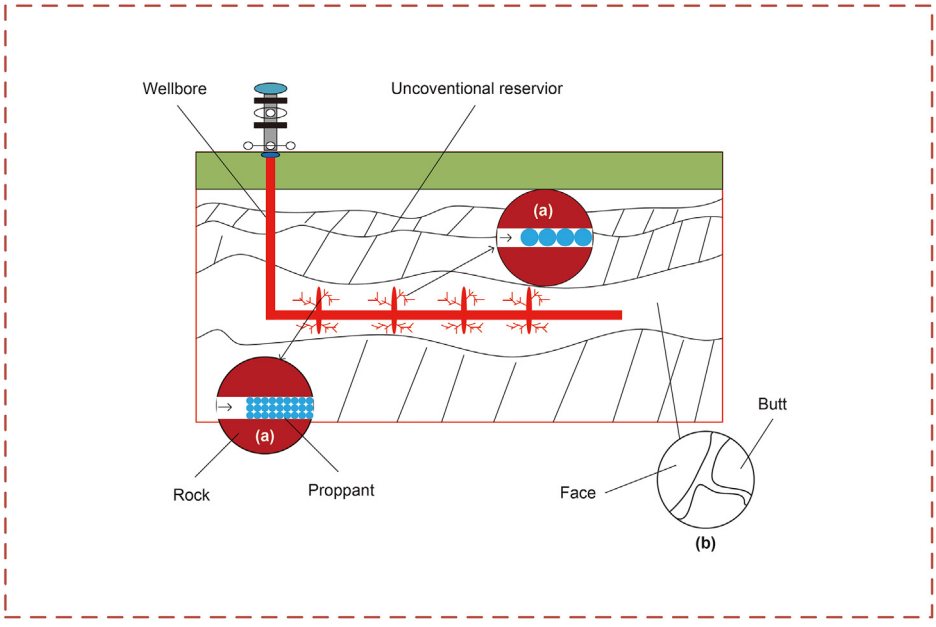


Fig. 1. Existence form of proppants in the reservoir.

$$d\varepsilon_{vs} = \frac{db_s}{b_s} \tag{3}$$

By substituting Eq. (3) into Eq. (2), the relationship between the soft part of the fracture and stress during the stress loading process can be obtained as:

$$b_s = b_{0s}\exp\left(-\frac{\sigma_e}{K_s}\right) \tag{4}$$

Similarly, for the fracture deformation in the hard part, the relationship between the stress and the strain can be described by the engineering strain based Hooke law:

$$d\sigma_e = K_h d\varepsilon_{vh} \tag{5}$$

where K_h is the modulus of hard part; and ε_{vh} is the volume strain in the hard part.

The volumetric strain in the hard fracture can also be expressed by the incremental change in the fracture width (Liu et al., 2009; Shang et al., 2019):

$$d\varepsilon_{vh} = \frac{db_h}{b_h} \tag{6}$$

Based on Eqs. (5) and (6), the fracture width of the hard part during the stress loading process is:

$$b_h = b_{0h}\left(1-\frac{\sigma_e}{K_h}\right) \tag{7}$$

Studies have shown that the hard part of the fracture has been normally regarded as a rigid body ($1/K_h << 1$) owing to its ample modulus (Shang et al., 2019). Therefore, under stress, the fracture width of shale can be expressed as:

$$b = b_{0h} + b_{0s}\exp\left(-\frac{\sigma_e}{K_s}\right) \tag{8}$$

The effective stress can be described by Biot's law as (Liu et al., 2017):

$$\sigma_e = \sigma_c - \gamma p \tag{9}$$

where σ_e is the external stress; γ is Biot's coefficient; σ_c is the confining pressure; and p is the pore pressure.

Permeability in shale is extremely low, and hydraulic fracturing techniques have been commonly used to improve permeability to increase shale gas production. During this process, it is important to understand the influence of the proppant on fracture width. Assumptions: (1) the shale fracture system is filled with part of a single layer of the proppant; (2) the proppant and the formation rock are both linear elastic spheres; (3) each proppant particle in the fracture bears a similar closing pressure; (4) the fractured rock is larger than the representative basic volume; (5) fracture closure is an elastic deformation process with negligible plastic deformation and rock/proppant failure. Therefore, continuum mechanics is applicable to examine those features in this instance. As shown in Fig. 3, part of the proppant is positioned in the fracture channel in the form of a single layer. When stress is applied, the embedding and deformation of a single proppant particle is shown in Fig. 3(b).

Similar to previous studies, in the process of proppant compaction and embedding, any change in fracture width caused by proppant deformation can be expressed as (Li et al., 2015; Liu et al., 2021):

$$\xi = 1.04D_1\left(K^2\sigma_e\frac{1-\nu_1^2}{E_1}\right)^{\frac{2}{3}} \tag{10}$$

where ξ is the proppant deformation; K is the distance coefficient; D_1 is the diameter of the proppant; ν_1 is Poisson's ratio of the proppant; and E_1 is the elastic modulus of the proppant.

In addition, during the stress loading process, the embedding depth of the proppant can be expressed as (Li et al., 2015; Liu et al., 2021):

$$h = 1.04D_1\left(K^2\sigma_e\right)^{\frac{2}{3}}\left[\left(\frac{1-\nu_1^2}{E_1}+\frac{1-\nu_2^2}{E_2}\right)^{\frac{2}{3}}-\frac{1-\nu_1^2}{E_1}\right] \tag{11}$$

where h is the value of embedment; E_2 is the elastic modulus of rock; and ν_2 is Poisson's ratio of rock.

In this work, our research interest was to determine the key factors affecting the fracture width of supporting fractures. So here we only analyzed changes in shale fracture deformation under the combined effects of stress and proppant. Therefore, under the combined action of proppants and stress, the fracture deformation in shale can be expressed as:

$$\Delta\varepsilon_p = \frac{b_{0h} + b_{0s}\exp\left(-\frac{\sigma_e}{K_s}\right) - 2(\xi+h)}{b_0} \tag{12}$$

In fact, whether it was a single micro-fracture, or a fracture network under reservoir conditions, the proportion of the hard part of the fracture would be very small, but would possess high roughness (Chen et al., 2012; Shang et al., 2019). Moreover, our research interest was mainly concerned with effective seepage channels, so b_{0h}/b_0 could be ignored in Eq. (12). And, under the combined action of stress and proppant, the deformation of the fracture could be expressed as:

$$\Delta\varepsilon_p = \exp\left(-\frac{\sigma_e}{K_s}\right) - \frac{2(\xi+h)}{b_0} = \exp\left(-\frac{\sigma_e}{K_s}\right) - \frac{2.08D_1\left(K^2\sigma_e\right)^{\frac{2}{3}}\left(\frac{1-\nu_1^2}{E_1}+\frac{1-\nu_2^2}{E_2}\right)\Big)^{\frac{2}{3}}}{b_0} \tag{13}$$

Wherein, the ratio of D_1/b_0 is related to the packing format of the proppant, which could be further expressed as (Xu et al., 2020):

$$c_0 = 1 + \frac{D_1}{b_0} \tag{14}$$

where c_0 represents the proppant packing format.

2.2. The change mechanism relating to shale fracture compressibility under a single proppant embedment

Fracture compressibility is one of the important parameters that determine changes in shale permeability, and is usually related to changes in stress. First, the fracture compressibility factor can be expressed as (Lu et al., 2016):

$$C_f = \frac{1}{K_f} = \frac{1}{K_s} \tag{15}$$

However, the fracture compressibility coefficient is not a constant value, but a function related to stress. In the past, the calculation method for the fracture compressibility coefficient is shown in Table 1.

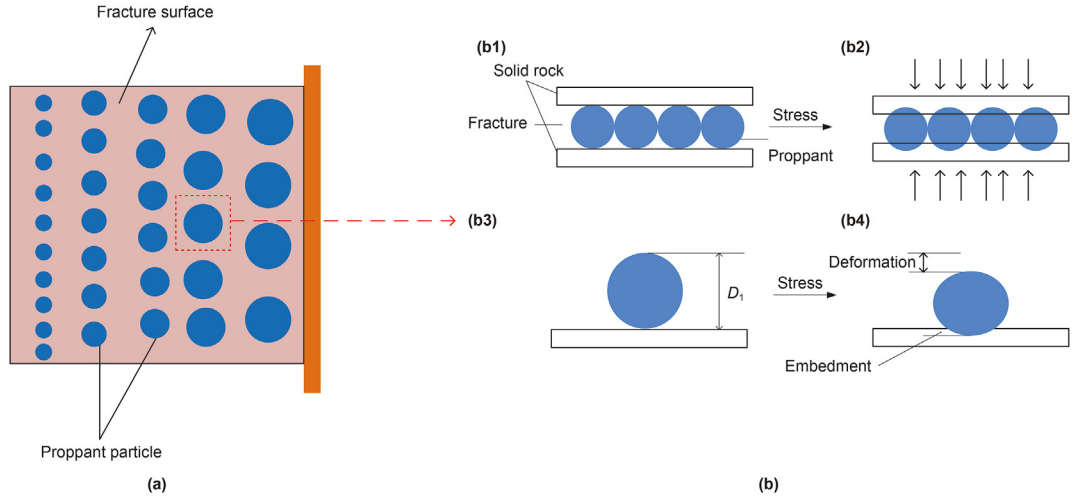


Fig. 3. Schematic diagram of the fracture system under a single layer of partial proppants. (**a**) Distribution of the proppants; (**b**) process of proppant embedment (after Liu et al., 2021).

Table 1
Review of the characterization methods of fracture compressibility.

Calculation model	Parameter	Remarks	Source
$\overline{C_f} = \frac{C_{f0}}{\alpha\Delta\sigma_e}[1-\exp(-\alpha\Delta\sigma_e)]$	C_{f0} is the initial fracture compressibility; α is the rate of decline of fracture compressibility; $\Delta\sigma_e$ is effective stress increases	Regression based on experimental data	Mckee et al. (1988)
$\overline{C_f} = \frac{a}{\sigma-\sigma_0}\int_{\sigma_0}^{\sigma}\frac{a}{\sigma+b}d\sigma$	a is the volume of the compressible pore under initial stress condition; b is the volume of the incompressible pore.	Calculation based on test data	Li et al. (2013)
$\overline{C_f} = \frac{C_0S_0+C_wS_w+C_p}{1-S_w}$	C_0 is the oil compressibility; S_0 is oil saturation; C_w is the water compressibility; S_w is the water saturation; C_p is the rock pore compressibility	Based on experimental data and theoretical calculations	Zhu et al. (2018)
$\overline{C_f} = \frac{\pi D_f\lambda_{min}^{3+\delta}\left(1-\frac{\sigma_e}{E}\right)^{3+\delta}L_0^{1-\delta}}{128\mu(3+\delta-D_f)\left[1+\frac{\sigma_e}{E}\right]}\left[\left(\frac{\lambda_{max0}}{\lambda_{min0}}\right)^{3+\delta-D_f}-1\right]$	λ_{max} is the maximum fracture spacing; D_f is the fractal dimension for the size distribution of crack spacing; δ is the capillary tortuosity fractal dimension; E is Young's modulus; λ_{max} is the minimum fracture spacing; μ is the gas viscosity	Based on experimental data and theoretical calculations	Cao et al. (2016)

In fact, the method of Mckee et al. (1988) has been commonly used in the modeling of fracture compressibility in coal or shale. Moreover, related studies have shown that this method could better fit the permeability changes in coal or shale under different stresses, and reflected the relationship between fracture compressibility and stress in shale or coal. Therefore, in this study, we still employed this method to describe the fracture compressibility changes in shale before the proppant was embedded. However, after the proppant was embedded, the fractures would be affected, and the depth of embedding would be related to stress. Therefore, in the process of proppant embedding, the fracture compression coefficient can be expressed as:

$$\overline{C_{fp}} = -\frac{1}{V_{fp}}\frac{dV_{fp}}{d\sigma_e} \tag{16}$$

where C_{fp} is the supported fracture compressibility; V_{fp} is the volume of the supported fracture.

Wherein, the volume of the supported fracture can be expressed as (Xu et al., 2020):

$$V_{fp} = A_f b\phi_f \tag{17}$$

where A_f represents the surface area of fracture, and ϕ_f the initial porosity of fracture.

Assuming that the contact area in the shale fracture was not affected by stress, Eq. (17) can be calculated to further transform the calculation method of the fracture compressibility into (Xu et al., 2020):

$$\overline{C_{fp}} = -\frac{1}{A_{fpb}\phi_f}\frac{d\left(A_{fpb}\phi_f\right)}{d\sigma_e} = -\frac{1}{\phi_f}\frac{d\phi_f}{d\sigma_e} - \frac{1}{b}\frac{db}{d\sigma_e} \tag{18}$$

In which, during the process of proppant embedding, changes in fracture porosity can be expressed by the following formula (Gangi, 1978):

$$\phi_f = \frac{\phi_{f0}\left[1-c_0\left(\frac{\sigma_e}{E_0}\right)^{\frac{2}{3}}\right]^3}{1-\phi_{f0}+\phi_{f0}\left[1-c_0\left(\frac{\sigma_e}{E_0}\right)^{\frac{2}{3}}\right]^3} \tag{19}$$

where E_0 is an equivalent modulus describing the mechanical interaction between two proppants in the proppant pack.

During this process, the first term of right hand side of Eq. (18), $-\frac{1}{\phi_f}\frac{d\phi_f}{d\sigma_e}$, can be expressed as:

$$-\frac{1}{\phi_f}\frac{d\phi_f}{d\sigma_e} = \frac{2c_0}{\sigma_e}\frac{\left(\frac{\sigma_e}{E_0}\right)^{\frac{2}{3}}}{1-c_0\left(\frac{\sigma_e}{E_0}\right)^{\frac{2}{3}}} \tag{20}$$

And, in the process of proppant embedding, $\frac{1}{b}\frac{db}{d\sigma_e}$ can be expressed as:

$$-\frac{1}{b}\frac{db}{d\sigma_e}=-\frac{1}{1-2(\xi+h)}\frac{d[1-2(\xi+h)]}{d\sigma_e}=\frac{1}{1-1.04\left(K^2\sigma_e\right)^{\frac{2}{3}}\left(\frac{1-\nu_1{}^2}{E_1}+\frac{1-\nu_2{}^2}{E_2}\right)^{\frac{2}{3}}(c_0-1)}\left\{1.386\left(K^2\sigma_e\right)^{-\frac{1}{3}}\left(\frac{1-\nu_1{}^2}{E_1}+\frac{1-\nu_2{}^2}{E_2}\right)^{\frac{2}{3}}(c_0-1)\right\} \tag{21}$$

Therefore, after proppant compaction and embedding, the fracture compressibility can be obtained by employing following formula:

$$\overline{C_{fp}}=\frac{2c_0}{\sigma_e}\frac{\left(\frac{\sigma_e}{E_0}\right)^{\frac{2}{3}}}{1-c_0\left(\frac{\sigma_e}{E_0}\right)^{\frac{2}{3}}}+\frac{1}{1-2.08\left(K^2\sigma_e\right)^{\frac{2}{3}}\left(\frac{1-\nu_1{}^2}{E_1}+\frac{1-\nu_2{}^2}{E_2}\right)^{\frac{2}{3}}(c_0-1)}\left\{1.386\left(K^2\sigma_e\right)^{-\frac{1}{3}}\left(\frac{1-\nu_1{}^2}{E_1}+\frac{1-\nu_2{}^2}{E_2}\right)^{\frac{2}{3}}(c_0-1)\right\} \tag{22}$$

2.3. The change mechanism in shale permeability compressibility under a single proppant embedment

When estimating shale permeability, it was usually thought necessary to consider the influence of the slippage effect (Klinkenberg, 1941):

$$k=k_a\left(1+\frac{B}{p}\right) \tag{23}$$

where k is permeability; k_a is the absolute permeability; B is the slippage factor.

From which, the value of the slippage factor determined the strength of the slippage effect, and changes in effective stress would directly lead to a change in the pore elasticity in the pore system by reducing or increasing the effective transmission aperture. Therefore, gas slip would be directly related to changes in the porelastic pore structure and effective stress (Fink et al., 2017):

$$B=B_0+\beta\sigma_e \tag{24}$$

where B_0 is the initial slippage factor; β is the slope of linear best fit, indicating the stress sensitivity of B.

Therefore, in the process of stress change, permeability that considered the effect of slippage could be construed as:

$$k=k_a\left(1+\frac{B_0+\beta\sigma_e}{p}\right) \tag{25}$$

However, when proppants are not injected, the absolute permeability in the shale reservoir can be calculated by applying cubic law. At this point, permeability that considered the effects of stress and slippage could be estimated by employing the following formula:

$$k=k_{a0}\left\{-3\frac{C_{f0}}{\alpha\sigma_e}[1-\exp(-\alpha\sigma_e)]\right\}\left(1+\frac{B_0+\beta\sigma_e}{p}\right) \tag{26}$$

where k_{a0} is the initial absolute permeability.

Similarly, during the embedding process of a proppant, shale permeability could be expressed as:

$$k=k_{a0}\left\{\exp\left(-\overline{C_{fp}}\sigma_e\right)-2.08D_1\left(K^2\sigma_e\right)^{\frac{2}{3}}\left(\frac{1-\nu_1{}^2}{E_1}+\frac{1-\nu_2{}^2}{E_2}\right)^{\frac{2}{3}}(c_0-1)\right\}^3\left(1+\frac{B_0+\beta\sigma_e}{p}\right) \tag{27}$$

3. Model verification and analysis

3.1. Changes in shale permeability under a single proppant embedment

Tan et al. (2018) conducted shale seepage experiments with different proppants under different positioning methods. Based on this experimental study, this study has selected permeability data under a single layer of a proppant in a single direction to verify the proposed permeability model. Based on this research, we preliminarily explored the change mechanism relating to shale permeability under a single layer of a proppant. The matching relationship between permeability and effective stress is shown in Fig. 4.

It can be seen from Fig. 4 that the permeability of shale decreased with an increase in effective stress under different pore pressures, no matter with or without a proppant. This is because shale fissures are compressible. In the process of increasing

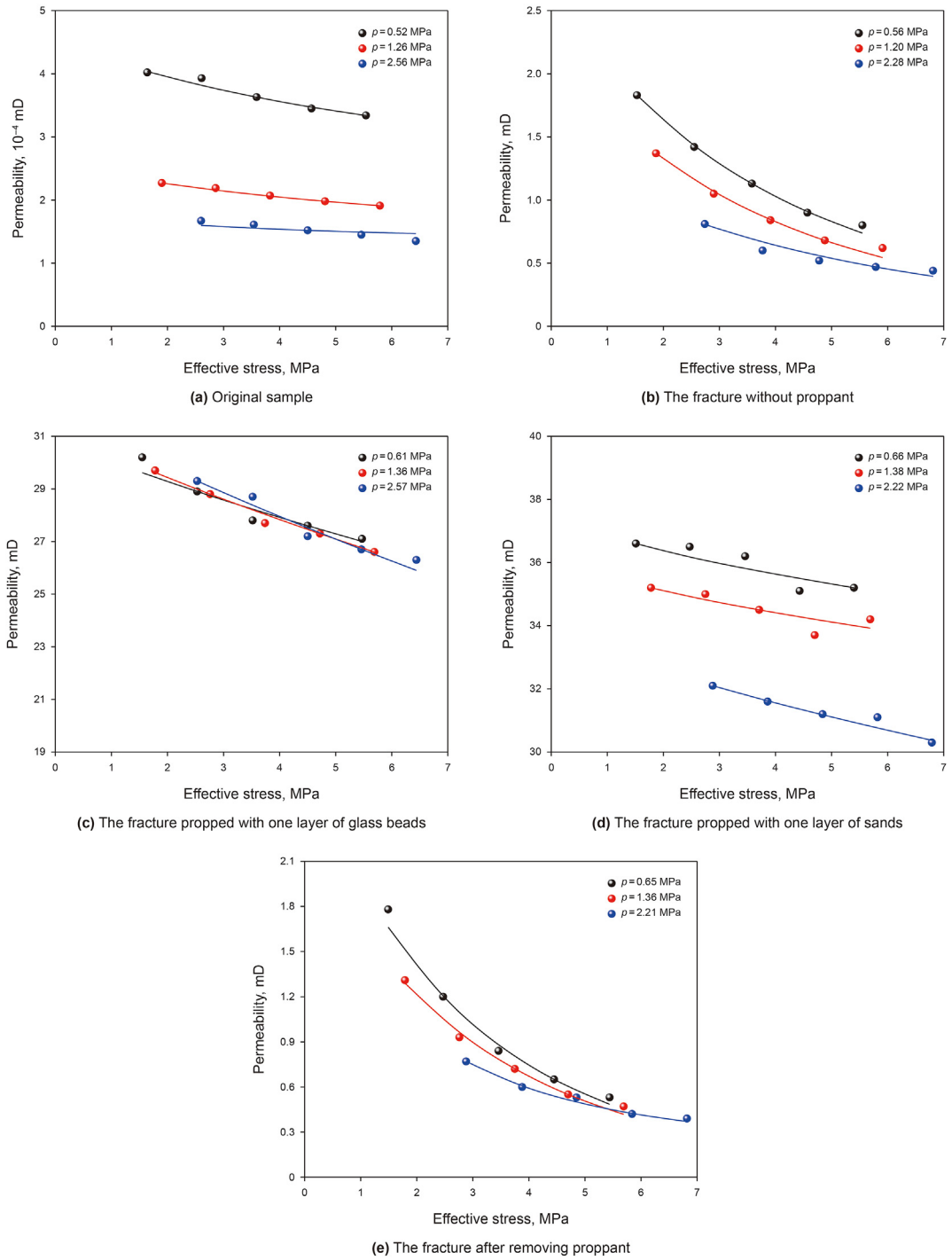


Fig. 4. The relationship between effective stress and permeability under different proppant placements (the solid line reflects the model calculation result).

Table 2
Model adopting parameters.

Parameter	Value	Source
Proppant packing format c_0, mm	2	Xu et al. (2020)
Young's modulus of rock matrix, GPa	25	Zhang et al. (2017)
Poisson's ratio of rock matrix	0.2	Zhang et al. (2017)
Young's modulus of glass bead, GPa	72	Xu et al. (2020)
Poisson's ratio of glass bead	0.2	Xu et al. (2020)
Young's modulus of sand, GPa	22.18	Wen et al. (2007)
Poisson's ratio of sand	0.35	Wen et al. (2007)
K	1	Li et al. (2015)

effective stress, shale fractures will be directly compressed (Chen et al., 2016). At this point, the seepage channel gradually decreases, resulting in a gradual decrease in permeability. However, after the proppant was embedded, the shale permeability was obviously greater than, previously, before the proppant was embedded (Tan et al., 2018). This was because, after the proppant had been placed, the shale fractures were supported by the proppant to achieve the effect of anti-reflection. Permeability, after removing the proppant, would be lower than that of the prefabricated fracture proppant. This would be the result, following

Table 3
Permeability modelling parameters.

Sample	k_{a0}, mD	B_0, MPa	β, MPa^{-1}	C_{f0}, MPa^{-1}	α
Original sample	1.201*10^{-4}	1.2	0.017	0.019	0.172
The fracture without proppant	1.186	0.344	0.152	0.082	0.026
The fracture propped with one layer of glass beads	26.997	0.291	−0.049	/	/
The fracture propped with one layer of sands	31.252	0.26	0.045	/	/
The fracture after removing proppant	1.696	0.464	0.168	0.158	0.152

Table 4
Compressibility coefficient of shale fracture under different proppant embedment (Tan et al., 2017).

Flow direction	Case	C_f, MPa^{-1}	Remarks
Horizontal 1	Case 1	0.088–0.17	The permeability of the original fracture along three principal directions was measured
	Case 2	0.017–0.11	The permeability of the fracture propped with proppant of 0.1 mm in average diameter, along two horizontal directions, was measured
	Case 3	0.061 −0.080	The permeability of the fracture after removal of the previous proppant along two horizontal directions was measured
	Case 4	0.040 −0.074	The permeability of the fracture propped with proppant of 0.539 mm in average diameter, along two horizontal directions, was measured.
Horizontal 2	Case 1	0.033 −0.045	/
	Case 2	0.018 −0.038	/
	Case 3	0.044–0.18	/
	Case 4	0.082 −0.085	/

the proppant support, the fracture structure would be damaged. During the process of removing the proppant, some of the fractures would heal automatically. In addition, it can be seen from the figure that the model calculation results were basically consistent with the test results. This shows that the model proposed in this paper could better simulate the change law relating to the shale permeability under proppant placement. From which, the parameters selected by the model in this paper are shown in Table 2.

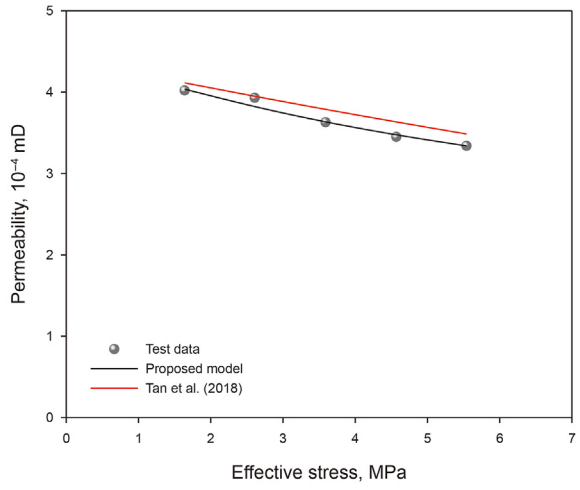
Because the influence of adsorption deformation has been ignored in this paper, the influence of the slippage effect still existed. Similar to previous studies (Tan et al., 2017, 2018), related parameters (the slippage effect, and initial absolute permeability) can be calculated by Eq. (27), as shown in Table 3.

Wu et al. (2018) believed that in order to compare the inherent flow capacity of rock media under different conditions, the gas slippage effect should be considered. It can be clearly seen from Table 3 that a smaller absolute permeability corresponded to a larger slippage factor. This was because the slippage factor was related to the pore and fracture structure, and had a significant negative correlation with permeability (Tan et al., 2017). The Klinkenberg constant B, which represents the gas slip effect, also changes with stress (Zhou et al., 2016). It is reported that as the effective stress increases, the compression of the pore structure narrows the pores in the rock, leading to more gas slippage (Letham and Bustin, 2016). Meanwhile, as the stress increases, the depth of embedment gradually increases, and the width of the fracture gradually decreases, the slippage effect will be more significant. The original shale sample was denser, and its compressibility was much smaller than that of fractured shale, which was inevitable. During this process, the fractured structure supported by the proppant would be destroyed, and the compressibility of the fracture would be greater than that in the fractured shale. Further, Tan et al. (2017) conducted an experimental study of the permeability and anisotropy of proppant-supported shale fractures. Among those, under the pressure embedding of different proppants, the variation range of the compressibility coefficient was obtained through calculation, as shown in Table 4. In another study by Tan et al. (2018): the compressibility of the original rock sample was 0.014 MPa^{-1}, the fractured shale 0.078 MPa^{-1}, and the single-layer glass bead-supported fractured shale 0.0093 MPa^{-1}, single-layer sand-supported fractured shale 0.0051 MPa^{-1}, and shale after proppant removal was 0.10 MPa^{-1}. Compared with Tan et al.'s research, the calculated values were similar in agreement with their results. However, the research in this paper further analyzed the change in the fracture compressibility coefficient during the effective stress change process, and further reflected on the change law of the fracture compressibility during the proppant embedding process.

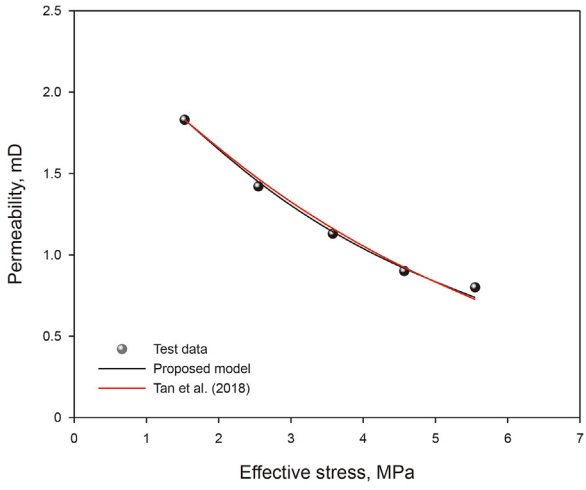
3.2. Comparison with model results of Tan et al. (2018)

Tan et al. (2018) conducted shale seepage experiments with different proppants under different positioning methods. Then, the permeability model of the combined effect of slippage effect and stress matched the data of the test results. Take the permeability data with effective stress of 1.64–5.54 MPa as an example. We compared the permeability model proposed in this paper with the research of Tan et al. (2018), as shown in Fig. 5.

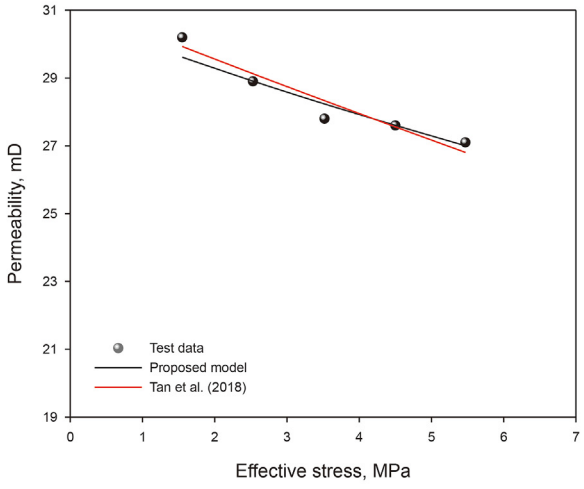
It can be seen from Fig. 5 that the permeability model proposed in this paper is basically consistent with the results of Tan et al. (2018). The described shale permeability all decreases with the increase in effective stress. However, compared with the study of Tan et al. (2018), the permeability model we proposed takes into account the influence of the heterogeneous characteristics of shale fractures, namely soft-hard fractures. Secondly, the proposed model also includes the effects of proppant compaction and embedding. At the same time, the model we proposed includes a fracture compressibility factor that takes into account the compaction and embedding effects of proppants, which can be used to describe changes in the compressibility of supported



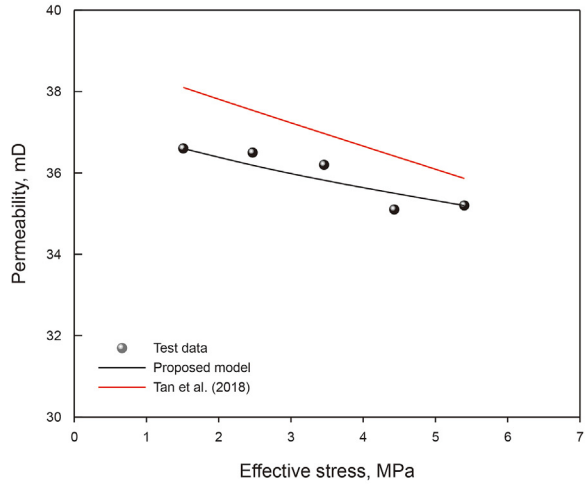
(a) Original sample



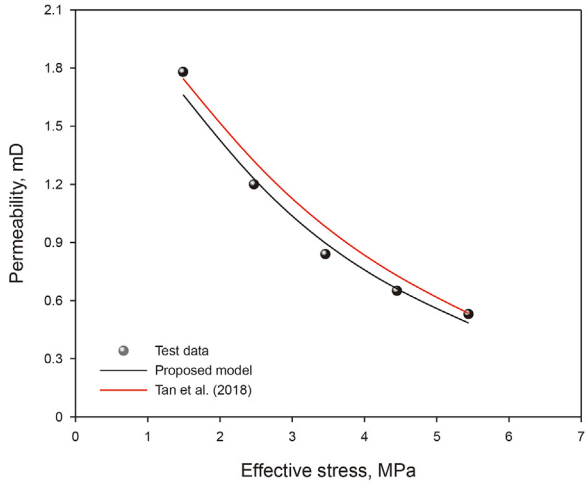
(b) The fracture without proppant



(c) The fracture propped with one layer of glass beads



(d) The fracture propped with one layer of sands



(e) The fracture after removing proppant

Fig. 5. Model comparison.

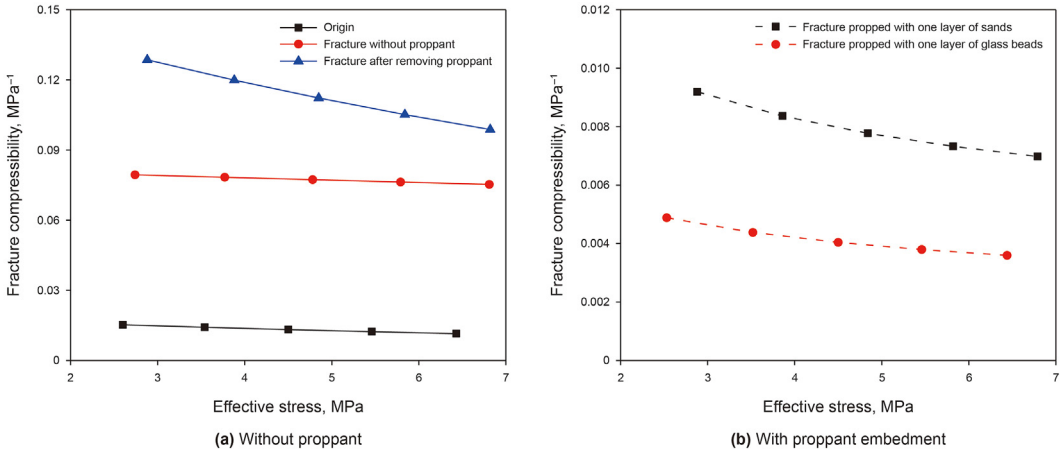


Fig. 6. Changes in compressibility of shale fractures before and after proppant embedding.

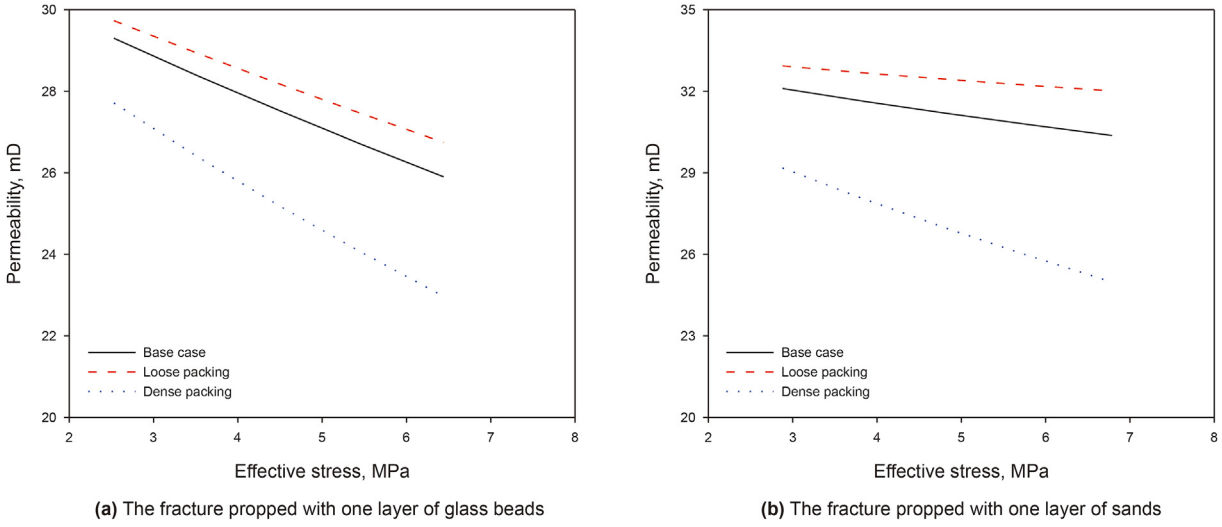


Fig. 7. Shale permeability under different packing forms of proppants.

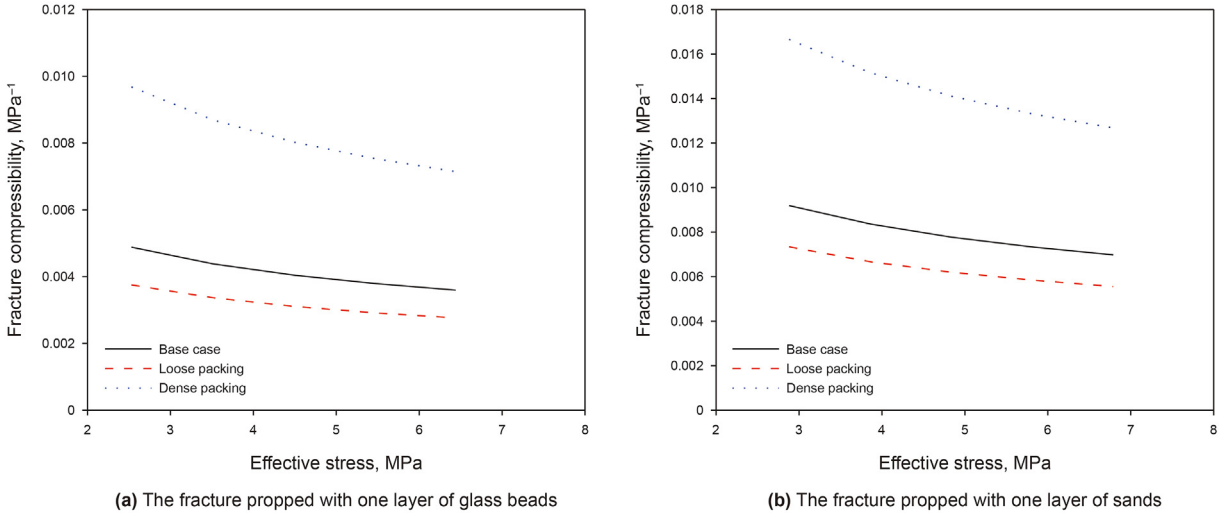


Fig. 8. Changes in compressibility of shale fractures with different packing forms of proppants.

fractures. In addition, we will consider the sress-dependent slippage effect into the proposed permeability model. However, the study of Tan et al. (2018) did not consider the impact of proppant embedding and compaction on the fracture and compressibility coefficient. When proppant is injected, the rock reservoir permeability and fracture compressibility may be an overestimation. Meanwhile, the permeability model proposed in this paper can be used to describe the influence of different proppants, different filling forms and different types of rocks on fracture permeability and compressibility coefficient.

3.3. Evolution of shale fracture compressibility under single proppant embedment

Based on the research method of Mckee et al. (1988) and Eq. (22), we calculated the evolution characteristics of the fracture compressibility before and after the proppant embedding, as shown in Fig. 6.

It can be seen from Fig. 6 that the compressibility coefficients of shale fractures all revealed a decreasing trend as effective stress increased. Owing to the influence of the proppant on the fracture structure, the fracture compression coefficient after proppant support was significantly greater than the fracture compression coefficients in the fractured shale and the original shale. But after embedding the proppant, its compressibility was smaller than that without the proppant. This was because the proppant supported fractures, and its compressibility changes depended on changes in the fracture width. And the change of fracture width is mainly affected by proppant deformation and embedding depth. (Ahamed et al., 2021). Therefore, shale had less compressibility during proppant embedding. In addition, the shale fracture compression factor when glass beads were embedded was smaller than that when sand was embedded. This was because the fracture compression coefficient usually decreased with an increase in the elastic modulus of proppants (Xu et al., 2020). The elastic modulus of glass beads was greater than that of sand, and the compressibility was smaller by comparison.

4. Discussion

4.1. The effect of the proppant packing form on permeability

The parameter that characterized the proppant packing form was c_0, which was similar to previous studies (Xu et al., 2020). The basic assumption in this paper was: $c_0 = 2$. We compared changes in permeability under the three packing forms of proppants, that were $c_0 = \sqrt{3}$ (loose packing), $c_0 = 2$ (base case), $c_0 = 2\sqrt{2}$ (dense packing), as shown in Fig. 7.

It can be seen from Fig. 7 that the permeability of different proppants under different packing forms decreased as the effective stress increased. At this point, a larger c_0 value corresponded to a smaller permeability, that was, the denser of the proppant placements, with smaller permeability. Initially, the filling form of the proppant affected fracture compressibility, because the rate of change in fracture porosity was one of the main determinants in the value of fracture compressibility, while the rate of change in fracture pore size played a secondary role: the larger the value of c_0, the greater the pore size, and the greater the rate of change, the greater the fracture compressibility. Previous studies have shown that a larger compressibility corresponded to a greater permeability (Tan et al., 2017). In addition, denser laying methods corresponded with larger embedding depths, resulting in reduced seepage channels and, consequently, reduced permeability.

4.2. The effect of the proppant packing form on fracture compressibility

On the one hand, the packing form of the proppant affected porosity and fracture space, and caused permeability changes. On the other hand, any change in fracture space caused fracture compressibility to change. Therefore, in the same way, we obtained the relationship between fracture compressibility and the effective stress when $c_0 = \sqrt{3}$ (loose packing), $c_0 = 2$ (base case), and $c_0 = 2\sqrt{2}$ (dense packing), as shown in Fig. 8.

It can be seen from Fig. 8 that with an increase in effective stress, the compressibility of shale fractures revealed a decreasing trend under different packing forms of different proppants. In the later stage of stress loading, a change in the compressibility coefficient gradually tended to be slight. In addition, the compressibility of shale fractures supported by sand was greater than that of glass bead supported fractures. This was mainly because the fracture compressibility was related to the change in fracture width and porosity. First, during the stress loading process, the depth of embedment gradually increased, directly compressing the fracture, but at the later stage, the degree of compression gradually inclined to its maximum, and later changes tended to be imperceptible (Chen et al., 2017). The elastic modulus of glass beads was greater than that of sand, which resulted in a change in the width of the fractures supported by glass beads, including a change in porosity that was smaller than that supported by sand. Moreover, different proppant filling methods produced different results, the compressibility of densely packed proppant fractures was greater than that of loosely packed fractured proppants. This was mainly because the filling form of the proppant determined the parameter c_0, which further affected the variation of fractures and porosity (Xu et al., 2020). Moreover, the gap width, including porosity changes, correlated with densely packed proppant fractures, which were greater than those of loosely packed proppants.

4.3. Characterization of the fracture compressibility and its permeability for coal under single proppant embedment

In order to explore the change mechanism relating to permeability and to the compressibility coefficient, when a proppant supported coal and rock fractures we used a similar method and combined the test data of Wu et al. (2018) to further carry out a comparative analysis, followed by discussion. From the results, without a proppant and single-layer proppant, the change law relating to the coal permeability during an effective stress change process is shown in Fig. 9.

Obviously, during the effective stress change loading process, changes in the coal permeability was almost the same as that of shale, and both decreased with an increase in effective stress. Further, the measured permeability value was basically consistent with the model calculation curve, which further confirmed that the model had good applicability for changes in permeability under the action of proppant compression. In addition, permeability, when the proppant was embedded, was considerably higher than that in the original coal sample, which was mainly the result of the effect of the proppant with respect to permeability improvement. Compared with shale, the elastic modulus in coal was much smaller, and the embedding depth of the proppant was larger at this point. Also, the fracture compression coefficient of the shale sample, which was also supported by glass beads, was significantly lower than that of coal. From the findings, the relationship between the fracture compressibility of the coal and effective stress has been depicted in Fig. 10.

It can be seen from Fig. 10 that the type of rock did not change the relationship between its compressibility coefficient and

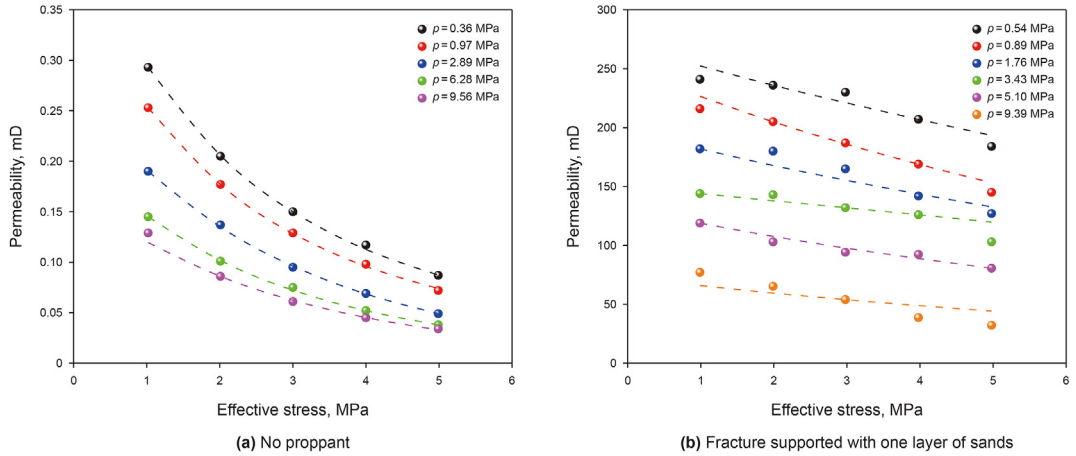


Fig. 9. The relationship between coal permeability and effective stress under proppant embedment.

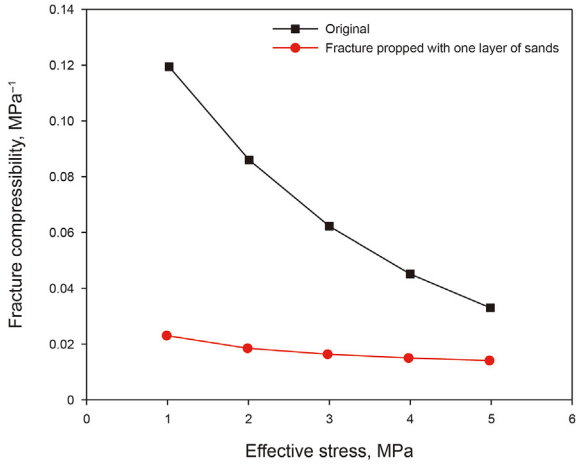


Fig. 10. Correspondence between coal compressibility coefficient and effective stress.

effective stress, because the compressibility coefficient was a function of effective stress. Because coal was softer and cracks were more sizeable, its permeability and compressibility coefficient were both greater than that of shale. Previous studies usually conducted seepage tests with methane as a fluid, leading to effective stresses changing during the test. The compressibility coefficients of coal were obtained based on different calculation methods, as shown in Table 5 (the listed compressibility coefficients were not affected by proppants; and the fluid was methane).

In addition, in the study of Wu et al., the compressibility of the original coal was 0.109 MPa^{-1}, and when supported by a single layer of glass beads, its value was 0.028 MPa^{-1} (Wu et al., 2018). From those findings, this study further analyzed the change mechanism of compressibility in the process of proppant compaction and embedment. Subsequently, changes in the coal permeability and the change law of compressibility under proppant compaction and embedment were analyzed, and constructed.

5. Limitations and prospects

In this work, we proposed a permeability model that considered the effect of a single proppant compaction and embedding in the heterogeneous fractures in shale. Further, based on changes in the shale fracture width, the calculation model of fracture compressibility under proppant compaction and embedding was further constructed. First of all, the calculation model of compressibility in this paper is only suitable for describing the compressibility of single-layer proppant-supported shale fractures. However, in actual situations, during hydraulic fracturing, the proppant in shale might be single layer or in multiple layers coexisting together. Therefore, it will be necessary to further explore changes in the shale permeability and the compressibility coefficient under the action of multi-layer proppants, which will be the focus of our next research project. Secondly, we assumed that the proppant was a linear elastic sphere, but, in fact, changes in the proppant in the shale reservoir may conceive a situation in which both elasticity and plasticity exist at the same time. Therefore, it will be necessary to explore thoroughly the influence of proppant embedding depth on permeability and the compressibility coefficient during the elastic or plastic process. Finally, the model was mainly based on a single fracture in a single direction, but shale has a high degree of heterogeneity. Therefore, it will be necessary to explore further the anisotropy of the shale fracture compression coefficient, including permeability. In addition, in order to investigate the differences in the influence of deep earth science and the *in-situ* environment of

Table 5
Summary of coal compressibility coefficients when no proppant was embedded.

Sample	Range of compressibility, MPa^{-1}	Source
Southern Sydney Basin, Australia	0.0366–0.0507	Chen et al. (2012)
Bowen Basin, Australia	0.0069–0.135	Connell et al. (2016)
Taroom coal measure, Surat Basin, Queensland, Australia	0.052–0.07	Gensterblum et al. (2014)
Jiulishan Coal Mine, Henan Province, China	0.051–0.077	Guo et al. (2017)
Southern Sydney Basin, Australia	0.0366–0.0507	Pan et al. (2010)
Chengzhuang coal mine in Qinshui Basin, China	0.016–0.19	Peng et al. (2017)
Yingjiahao, Luzhongde and Yushe coal mines in the Western Guizhou	Low rank: 0.0051–0.064 Medium rank: 0.0152–0.0172 High rank: 0.0051–0.0092	Li et al. (2013)
Leichhardt seam, northern Bowen Basin, Queensland	0.064–0.13	Peng et al. (2017)

different occurrence depths on the physical and mechanical behavior of rocks, Xie et al. (2021) proposed the definition and connotation of the concept of "deep *in-situ* rock mechanics" to further analyze the mechanical properties of deep rocks. Therefore, it is necessary to carry out further research on the seepage characteristics of rock which supported by proppants with different formation conditions and different depths.

6. Conclusions

In this paper, based on the heterogeneous structure of shale fractures, we proposed a permeability model that considered the combined effects of proppant and stress during hydraulic fracturing. Moreover, the influence of the slippage effect was included in the permeability model, and its rationality was verified through publicly released test data. From the findings, the calculation model of fracture compressibility under proppant compaction and embedding during hydraulic fracturing was further constructed. The main results and conclusions are as follows:

(1) In the process of hydraulic fracturing, when a proppant supports a fracture, the change in the fracture width is mainly controlled by the proppant deformation and embedding depth. The embedding depth of the proppant and the deformation of the proppant was found to be related to stress. The embedding depth and the deformation of the proppant increased with an increase in stress, and the fracture width gradually closed during the process.

(2) Whether proppants are injected or not does not change the relationship between stress and permeability, i.e. there exists a negative correlation between stress and permeability. Because, in the process of an increase in stress, shale fractures tended to close, and during this process, the proppant embedding depth and proppant deformation both showed an increasing trend, then the permeability decreased accordingly. Owing to the supporting effect of the proppant, the fracture permeability which propped by proppants was much higher than that of shale in its original state. In addition, the evolution of shale permeability is also restricted by the type of proppant, packing mode and rock mechanical properties. Among them, for the same type of rock, the permeability of fractures supported by proppants with a smaller elastic modulus supports greater. And the tighter the proppants are arranged, the lower the permeability.

(3) Fracture compressibility was one of the key parameters that determined gas flow in shale reservoirs, and its change was mainly determined by the changes in fracture width and porosity. Therefore, the compressibility coefficient of the supported fracture changes under the action of stress. This means that the fracture compressibility coefficient mainly depends on the mechanical properties of the rock, the type of proppant and the packing mode of the proppants. Wherein, in the same reservoir, a proppant with larger elastic modulus corresponded with a smaller fracture compressibility. Secondly, under similar proppant support, a rock with a larger elastic modulus was analogous to a smaller fracture compressibility. Finally, in the same reservoir, the fracture compressibility coefficient of a densely packed proppant was larger.

Acknowledgments

This study was financially supported by the National Natural Science Foundation of China (Grants No. 52064007, 51804085, and 51911530203) and supported by Guizhou Provincial Science and Technology Projects (Qianke Combination Foundation-ZK[2021] Key 052).

References

Ahamed, A., Perera, S., Black, J.R., Matthai, S.K., Hewage, S., 2021. Investigating the proppant damage mechanisms expected in a propped coal fracture and its effect on fracture flow. J. Petrol. Sci. Eng. 198, 108170. https://doi.org/10.1016/j.petrol. 2020.108170.

Ahamed, M., Perera, S., Li, D.Y., Ranjith, P.G., Matthai, S.K., 2019. Proppant damage mechanisms in coal seam reservoirs during the hydraulic fracturing process: a review. Fuel 253, 615–629. https://doi.org/10.1016/j.fuel.2019.04.166.

Bandara, K.M.A.S., Ranjith, P.G., Rathnaweera, T.D., 2019. Improved understanding of proppant embedment behavior under reservoir conditions: a review study. Powder Technol. 352, 170–192. https://doi.org/10.1016/j.powtec.2019.04.033.

Cao, H.T., Yi, X.Y., Lu, Y., Xiao, Y., 2016. A fractal analysis of fracture conductivity considering the effects of closure stress. J. Nat. Gas Sci. Eng. 32, 549–555. https://doi.org/10.1016/j.jngse.2016.04.022.

Chen, Z., Liu, J., Pan, Z., Connell, L.D., Elsworth, D., 2012. Influence of the effective stress coefficient and sorption-induced strain on the evolution of coal permeability: model development and analysis. Int. J. Greenh. Gas Control 8, 101–110. https://doi.org/10.1016/j.ijggc.2012.01.015.

Chen, D., Pan, Z., Ye, Z., 2015. Dependence of gas shale fracture permeability on effective stress and reservoir pressure: model match and insights. Fuel 139, 383–392. https://doi.org/10.1016/j.fuel.2014.09.018.

Chen, D., Pan, Z., Ye, Z., Hou, B., Yuan, L., 2016. A unified permeability and effective stress relationship for porous and fractured reservoir rocks. J. Nat. Gas Sci. Eng. 29, 401–412. https://doi.org/10.1016/j.jngse.2016.01.034.

Chen, D., Ye, Z., Pan, Z., Zhou, Y., Zhang, J., 2017. A permeability model for the hydraulic fracture filled with proppant packs under combined effect of compaction and embedment. J. Petrol. Sci. Eng. 149, 428–435. https://doi.org/10.1016/j.petrol.2016.10.045.

Chen, T., Feng, X.T., Cui, G., Tan, Y., Pan, Z., 2019. Experimental study of permeability change of organic-rich gas shales under high effective stress. J. Nat. Gas Sci. Eng. 64, 1–14. https://doi.org/10.1016/j.jngse.2019.01.014.

Connell, L.D., Mazumder, S., Sander, R., Camilleri, M., Pan, Z., Heryanto, D., 2016. Laboratory characterisation of coal matrix shrinkage, cleat compressibility and the geomechanical properties determining reservoir permeability. Fuel 165, 499–512. https://doi.org/10.1016/j.fuel.2015.10.055.

Estrada, J.M., Bhamidimarri, R., 2016. A review of the issues and treatment options for waste water from shale gas extraction by hydraulic fracturing. Fuel 182, 292–303. https://doi.org/10.1016/j.fuel.2016.05.051.

Feng, R., Harpalani, S., Pandey, R., 2016. Laboratory measurement of stress-dependent coal permeability using pulse-decay technique and flow modeling with gas depletion. Fuel 177, 76–86. https://doi.org/10.1016/j.fuel.2016.02.078, 2016.

Fink, R., Krooss, B.M., Gensterblum, Y., Amann-Hildenbrand, A., 2017. Apparent permeability of gas shales–superposition of fluid-dynamic and poro-elastic effects. Fuel 199, 532–550. https://doi.org/10.1016/j.fuel.2017.02.086.

Gale, J.F.W., Laubach, S.E., Olson, J.E., Eichhubi, P., Fall, A., 2014. Natural fractures in shale: a review and new observations. AAPG Bull. 98 (11), 2165–2216. https://doi.org/10.1306/08121413151.

Gangi, A.F., 1978. Variation of whole and fractured porous rock permeability with confining pressure. Int. J. Rock Mech. Min. Sci. Geomech. Abstr. 15 (5), 249–257. https://doi.org/10.1016/0148-9062(78)90957-9.

Gao, Q., Han, S.C., Cheng, Y., Li, Y., Han, Z., 2020. Apparent permeability model for gas transport through micropores and microfractures in shale reservoirs. Fuel 285, 119086. https://doi.org/10.1016/j.fuel.2020.119086.

Gensterblum, Y., Ghanizadeh, A., Krooss, B.M., 2014. Gas permeability measurements on Australian subbituminous coals: fluid dynamic and poroelastic aspects. J. Nat. Gas Sci. Eng. 19, 202–214. https://doi.org/10.1016/j.jngse.2014.04.016.

Guo, J., Liu, Y., 2012. Modeling of proppant embedment: elastic deformation and creep deformation. In: SPE International Production and Operations Conference & Exhibition. https://doi.org/10.2118/157449-MS.

Guo, J., Qin, Q., Zhang, R., 2017. Evaluation of the damages of permeability and effective porosity of tectonically deformed coals. Arabian J. Geosci. 10, 357. https://doi.org/10.1007/s12517-017-3140-8.

Guo, X., Yao, Y., Liu, D., 2014. Characteristics of coal matrix compressibility: an investigation by mercury intrusion porosimetry. Energy Fuels 28, 3673–3678. https://doi.org/10.1021/ef5004123.

Hon, C.L., Adiyodi, V.R., Seeram, R., 2019. Maximizing production from shale reservoir by using micro-sized proppants. In: International Petroleum Technology Conference. https://doi.org/10.2523/IPTC-19437-MS.

Hou, L., Elsworth, D., 2021. Mechanisms of tripartite permeability evolution for supercritical CO_2 in propped shale fractures. Fuel 292, 120188. https://doi.org/10.1016/j.fuel.2021.120188.

Keshavarza, A., Badalyan Jr., Bedrikovetsky, R.J., 2016. Productivity enhancement by stimulation of natural fractures around a hydraulic fracture using micro-sized proppant placement. J. Nat. Gas Sci. Eng. 33, 1010–1024. https://doi.org/10.1016/j.jngse.2016.03.065.

Khanna, A., Keshavarz, A., Mobbs, K., Davis, M., Bedrikovetsky, P., 2013. Stimulation of the natural fracture system by graded proppant injection. J. Petrol. Sci. Eng.

111, 71–77. https://doi.org/10.1016/j.petrol.2013.07.004.
Klinkenberg, L.J., 1941. The permeability of porous media to liquid and gases. API Drill. Prod. Prac 200–213. https://doi.org/10.1016/0148-9062(41)90957-9.
Letham, E.A., Bustin, R.M., 2016. The impact of gas slippage on permeability effective stress laws: implications for predicting permeability of fine-grained lithologies. Int. J. Coal Geol. 167, 93–102. https://doi.org/10.1016/j.coal.2016.09.015.
Li, K., Gao, Y., Lyu, Y., Wang, M., 2015. New mathematical models for calculating proppant embedment and fracture conductivity. SPE J. 20, 496–507. https://doi.org/10.2118/155954-PA.
Li, S., Tang, D., Pan, Z., Xu, H., Huang, W., 2013. Characterization of the stress sensitivity of pores for different rank coals by nuclear magnetic resonance. Fuel 111, 746–754. https://doi.org/10.1016/j.fuel.2013.05.003.
Liu, H., Bedrikovetsky, P., Yuan, Z., Liu, Jv, Liu, Y., 2021. An optimized model of calculating optimal packing ratio for graded proppant placement with consideration of proppant embedment and deformation. J. Petrol. Sci. Eng. 196, 107703. https://doi.org/10.1016/j.petrol.2020.107703.
Liu, H.H., Rutqvist, J., Berryman, J.G., 2009. On the relationship between stress and elastic strain for porous and fractured rock. Int. J. Rock Mech. Min. Sci. 46 (2), 289–296. https://doi.org/10.1016/j.ijrmms.2008.04.005.
Liu, J., Chen, Z., Elsworth, D., Qu, H., Chen, D., 2011. Interactions of multiple processes during CBM extraction: a critical review. Int. J. Coal Geol. 87 (3–4), 175–189. https://doi.org/10.1016/j.coal.2011.06.004.
Liu, T., Lin, B., Wei, Y., 2017. Impact of matrix-fracture interactions on coal permeability: model development and analysis. Fuel 207, 522–532. https://doi.org/10.1016/j.fuel.2017.06.125.
Lu, S., Cheng, Y., Li, W., 2016. Model development and analysis of the evolution of coal permeability under different boundary conditions. J. Nat. Gas Sci. Eng. 31, 129–138. https://doi.org/10.1016/j.jngse.2016.02.049.
Lv, Q., Shi, J., Ranjith, P.G., 2020. Effects of testing method, lithology and fluid-rock interactions on shale permeability: a review of laboratory measurements. J. Nat. Gas Sci. Eng. 78, 103302. https://doi.org/10.1016/j.jngse.2020.103302.
McGlade, C., Speirs, J., Sorrell, S., 2013. Unconventional gas – a review of regional and global resource estimates. Energy 55, 571–584. https://doi.org/10.1016/j.energy.2013.01.048.
Mckee, C.R., Bumb, A.C., Koenlg, R.A., 1988. Stress-dependent permeability and porosity of coal and other geologic formations. SPE Form. Eval. 3, 81–91. https://doi.org/10.2118/12858-PA.
Meng, Z., Li, G., 2013. Experimental research on the permeability of high-rank coal under a varying stress and its influencing factors. Eng. Geol. 162, 108–117. https://doi.org/10.1016/j.enggeo.2013.04.013.
Pan, L., Jones, S.J., Wang, X., Guan, W., Li, L., 2019. Re-evaluation of the porosity measurements under different confining pressures: a better appraisal of reservoir porosity. AAPG Bull. 103 (3), 515–526. https://doi.org/10.1306/09181817131.
Pan, Z., Connell, L.D., 2012. Modelling permeability for coal reservoirs: a review of analytical models and testing data. Int. J. Coal Geol. 92, 1–44. https://doi.org/10.1016/j.coal.2011.12.009.
Pan, Z., Connell, L.D., Camilleri, M., 2010. Laboratory characterisation of coal reservoir permeability for primary and enhanced coalbed methane recovery. Int. J. Coal Geol. 82, 252–261. https://doi.org/10.1016/j.coal.2009.10.019.
Pan, Z., Ma, Y., Connell, L.D., Down, D.I., Camilleri, M., 2015. Measuring anisotropic permeability using a cubic shale sample in a triaxial cell. J. Nat. Gas Sci. Eng. 26, 336–344. https://doi.org/10.1016/j.jngse.2015.05.036.
Pei, S., Wang, X., Yu, S., Li, Y., 2018. Study on the characteristics of matrix compressibility and its influence factors for different rank coals. J. Nat. Gas Sci. Eng. 56, 93–106. https://doi.org/10.1016/j.jngse.2018.05.035.
Peng, S., Fang, Z., Shen, J., Xu, J., Wang, G., 2017. Effects of gas sorption-induced swelling/shrinkage on the cleat compressibility of coal under different bedding directions. Sci. Rep. 7, 14337. https://doi.org/10.1038/s 41598-017-14678-1.
Robertson, E.P., Christiansen, R.L., 2006. A permeability model for coal and other fractured, sorptive-elastic media. SPE J. 13 (3), 314–324. https://doi.org/10.2118/104380-PA.
Seidle, J.P., Jeansonne, D.J., Erickson, D.J., 1992. Application of matchstick geometry to stress dependent permeability in coals. In: SPE Rocky Mountain Regional Meeting. https://doi.org/10.2118/24361-MS.
Seidle, J.R., Huitt, L.G., 1995. Experimental measurement of coal matrix shrinkage due to gas desorption and implications for cleat permeability increases. In: International Meeting on Petroleum Engineering. https://doi.org/10.2118/30010-MS.
Shang, X.J., Wang, J.G., Zhang, Z., Gao, F., 2019. A three-parameter permeability model for the cracking process of fractured rocks under temperature change and external loading-sciencedirect. Int. J. Rock Mech. Min. Sci. 123, 104106. https://doi.org/10.1016/j.ijrmms.2019.104106.
Shi, J.Q., Durucan, S., 2010. Exponential growth in San Juan Basin Fruitland coalbed permeability with reservoir drawdown: model match and new insights. SPE Reservoir Eval. Eng. 13, 914–925. https://doi.org/10.2118/123206-PA.
Tan, Y., Pan, Z., Feng, X.T., Connell, L.D., 2018. Laboratory study of proppant on shale fracture permeability and compressibility. Fuel 222, 83–97. https://doi.org/10.1016/j.fuel.2018.02.141.
Tan, Y., Pan, Z., Feng, X.T., Zhang, D., Li, S., 2019. Laboratory characterisation of fracture compressibility for coal and shale gas reservoir rocks: a review. Int. J. Coal Geol. 204, 1–17. https://doi.org/10.1016/j.coal.2019.01.010.
Tan, Y., Pan, Z., Liu, J., Wu, Y., Connell, L.D., 2017. Experimental study of permeability and its anisotropy for shale fracture supported with proppant. J. Nat. Gas Sci. Eng. 44, 250–264. https://doi.org/10.1016/j.jngse.2017.04.020.
Warpinski, N.R., Mayerhofer, M.J., Vincent, M.C., Cipolla, C.L., Lolon, E.P., 2008. Stimulating unconventional reservoirs: maximizing network growth while optimizing fracture conductivity. In: SPE Unconventional Reservoirs Conference. https://doi.org/10.2118/114173-MS.
Wang, C., Zhang, J., Chen, J., Zhong, R., Chen, Z., 2021. Understanding competing effect between sorption swelling and mechanical compression on coal matrix deformation and its permeability. Int. J. Rock Mech. Min. Sci. 138, 104639. https://doi.org/10.1016/j.ijrmms.2021.104639.
Wei, M., Liu, J., Elsworth, D., Li, S., Zhou, F., 2019. Influence of gas adsorption induced non-uniform deformation on the evolution of coal permeability. Int. J. Rock Mech. Min. Sci. 114, 71–78. https://doi.org/10.1016/j.ijrmms.2018.12.021.
Wei, M., Liu, J., Elsworth, D., Liu, Y., Zeng, J., He, Z., 2021. Impact of equilibration time lag between matrix and fractures on the evolution of coal permeability. Fuel 290, 120029. https://doi.org/10.1016/j.fuel.2020.120029.
Wei, W., Xia, Y., 2017. Geometrical, fractal and hydraulic properties of fractured reservoirs: a mini-review. Adv Geo-Energy Res. 1, 31–38. https://doi.org/10.26804/ager.2017.01.03.
Wen, Q., Zhang, S., Wang, L., Liu, Y., Li, X., 2007. The effect of proppant embedment upon the long-term conductivity of fractures. J. Petrol. Sci. Eng. 55, 221–227. https://doi.org/10.1016/j.petrol.2006.08.010.
Wu, Y., Pan, Z., Zhang, D., David, I.D., Lu, Z.H., Connell, L.D., 2018. Experimental study of permeability behaviour for proppant supported coal fracture. J. Nat. Gas Sci. Eng. 51, 18–26. https://doi.org/10.1016/j.jngse.2017.12.023.
Xie, H., Li, C., He, Z., Li, C., Lu, Y., Zhang, R., Gao, F., 2021. Experimental study on rock mechanical behavior retaining the in situ geological conditions at different depths. Int J Rock Mech Min 138, 104548. https://doi.org/10.1016/j. ijrmms.2020.104548.
Xu, Y., Ezulike, O., Dehghanpour, H., 2020. Estimating compressibility of complex fracture networks in unconventional reservoirs. Int. J. Rock Mech. Min. Sci. 127 (7), 104186. https://doi.org/10.1016/j.ijrmms.2019.104186.
Yang, L., Ge, H., Shen, Y., Zhang, J., Yan, W., Wu, S., et al., 2015. Imbibition inducing tensile fractures and its influence on in-situ stress analyses: a case study of shale gas drilling. J. Nat. Gas Sci. Eng. 26, 927–939. https://doi.org/10.1016/j.jngse.2015.07.028.
Zeng, J., Liu, J., Li, W., Guo, J., 2021. A process-based coal swelling model: bridging the gaps between localized swelling and bulk swelling. Fuel 293, 120360. https://doi.org/10.1016/j.fuel.2021.120360.
Zeng, J., Liu, J., Li, W., Leong, Y.K., Elsworth, D., Guo, J., 2020a. Evolution of shale permeability under the influence of gas diffusion from the fracture wall into the matrix. Energy Fuels 34 (4), 4393–4406. https://doi.org/10.1021/acs. energyfuels. 0c00219.
Zeng, J., Liu, J., Li, W., Leong, Y.K., Guo, J., 2020b. Evolution of shale permeability under the influence of gas diffusion from the fracture wall into the matrix. Energy Fuels. https://doi.org/10.1021/acs.energyfuels.0c00219.
Zhang, J., Hou, J., 2016. Theoretical conductivity analysis of surface modification agent treated proppant II – channel fracturing application. Fuel 134, 166–170. https://doi.org/10.1016/j.fuel.2015.10.026.
Zhang, S., Sang, Q., Dong, M., 2021. Experimental study of pressure sensitivity in shale rocks: effects of pore shape and gas slippage. J. Nat. Gas Sci. Eng. 89, 103885. https://doi.org/10.1016/j.jngse.2021.103885.
Zhang, X., Wang, J.G., Gao, F., Ju, Y., Liu, J., 2017. Impact of water and nitrogen fracturing fluids on fracturing initiation pressure and flow pattern in anisotropic shale reservoirs. Comput. Geotech. 81, 59–76. https://doi.org/10.1016/j.compgeo. 2016.07.011.
Zhou, J., Zhang, L., Li, X., Pan, Z., 2019. Experimental and modeling study of the stress-dependent permeability of a single fracture in shale under high effective stress. Fuel 257, 116078. https://doi.org/10.1016/j.fuel.2019.116078.
Zhou, Y., Li, Z., Yang, Y., Zhang, L., Si, L., Kong, B., Li, J., 2016. Evolution of coal permeability with cleat deformation and variable Klinkenberg effect. Transport Porous Media 115 (1), 153–167. https://doi.org/10.1007/s11242-016-0759-y.
Zhu, S., Du, Z., Li, C., You, Z., Peng, X., 2018. Deng P. An analytical model for pore volume compressibility of reservoir rock. Fuel 232, 543–549. https://doi.org/10.1016/j.fuel.2018.05.165.